Capturing the complete stress–strain behaviour of jointed rock using a numerical approach

Kamran Esmaieli[1], John Hadjigeorgiou[1], and Martin Grenon[2]

[1]*Lassonde Institute of Mining, University of Toronto, Toronto, Canada*

[2]*Faculté des sciences et de génie, Département de génie des mines, de la métallurgie et des matériaux, Université Laval, Québec, Canada*

ABSTRACT

This paper presents the results of a series of numerical experiments using the synthetic rock mass (SRM) approach to quantify the behaviour of jointed rock masses. Field data from a massive sulphide rock mass, at the Brunswick mine, were used to develop a discrete fracture network (DFN). The constructed DFN model was subsequently subjected to random sampling whereby 40 cubic samples, of height to width ratio of two, and of varying widths (0.05 to 10 m) were isolated. The discrete fracture samples were linked to 3D bonded particle models to generate representative SRM models for each sample size. This approach simulated the jointed rock mass as an assembly of fractures embedded into the rock matrix. The SRM samples were submitted to uniaxial loading, and the complete stress–strain behaviour of each specimen was recorded. This approach provided a way to determine the complex constitutive behaviour of large-scale rock mass samples. This is often difficult or not possible to achieve in the laboratory. The numerical experiments suggested that higher post-peak modulus values were obtained for smaller samples and lower values for larger sample sizes. Furthermore, the observed deviation of the recorded post-peak modulus values decreased with sample size. The ratio of residual strength of rock mass samples per uniaxial compressive strength intact increases moderately with sample size. Consequently, for the investigated massive sulphide rock mass, the pre-peak and post-peak representative elemental volume size was found to be the same (7 × 7 × 14 m).

KEYWORDS

synthetic rock mass (SRM); discrete fracture network (DFN); stress–strain behaviour; jointed rock

CITATION

Esmaieli K, Hadjigeorgiou J, & Grenon M. (2015) Capturing the complete stress–strain behaviour of jointed rock using a numerical approach. International Journal for Numerical and Analytical Methods in Geomechanics (2015) 39(10), 1027-1044.

This is the author's version of the original manuscript. The final publication is available at Wiley Online library via **https://doi.org/10.1002/nag.2346**

1 INTRODUCTION

The mechanical behaviours of a jointed rock mass can differ from that of the constituent rock matrix. The presence and number of discontinuities or planes of weakness such as joints or bedding planes can result in a more complex behaviour. Although the determination of the mechanical properties of intact rock specimens, single discontinuities and granular materials in the laboratory is relatively straightforward, determination of the mechanical properties of a rock mass presents several challenges. Given the difficulties in conducting tests on large-scale rock mass mechanical properties, empirical rock mass classification methods such as the geological strength index (GSI)

[1], rock mass rating [2] and Q-system [3] are frequently used to extrapolate the mechanical behaviour of rock masses.

Depending on the size of an excavation within a rock mass (i.e. tunnel, stope, pillar, etc.), the mechanical behaviour of the rock mass can be different. This is often referred to as the scale effect. An indication of the behaviour of large rock mass samples can also be derived by extrapolating from small laboratory samples using some form of degradation to account for scale effect. This can be through the use of classification ratings or some more complex degradation strategies [4].

Empirical or numerical back-analyses of rock mass failure case studies can be also used to estimate the rock mass mechanical behaviour at large scale [5–7]. The majority of these analyses, however, are often based on the assumption that the rock mass is isotropic and homogeneous. This assumption is not always justifiable.

It is also noted that a large number of rock mechanics laboratories are only equipped to conduct tests that capture the peak loads of intact rock samples. The laboratories report the peak strength, elastic modulus and Poisson's ratio as well as the failure mechanism. Capturing the full stress strain behaviour of intact rock samples requires the use of very stiff and servo-controlled testing machines [8]. Consequently, in many cases, indirect empirical or numerical approaches are used to estimate the post-peak behaviours of rocks [9–15]. The post-peak behaviour of rock can be of importance in dictating the performance of underground excavations. Estimation of the range of plastic strain, over which the strain-softening response occurs, will indicate the conditions under which failure will take place (e.g. violent and sudden as opposed to progressive). A better understanding of this process can contribute in gaining an insight into the rockburst potential of deep and high stress mines.

An interesting approach to calibrate the elasto-plastic behaviour of 3D numerical models for an underground excavation has relied on the use of long-term micro-seismic records. Andrieux et al.

[12] matched regions of rock mass failure determined by the numerical model at different mining steps, with the corresponding recorded seismicity by varying peak strength and post-peak behaviour (strength softening) of the rock mass.

Cai et al. [11] demonstrated the critical influence of the residual strength on the yielding zone around a 6 m wide tunnel. The implication was that the residual strength of rock masses has to be properly determined in order to design appropriate rock support systems. Cai et al. [11] proposed the use of GSI to estimate the residual strength of rock masses. A similar approach has been employed by Alejano et al. [13, 14] where they defined the post failure behaviour of rock masses based on GSI values, Figure 1.

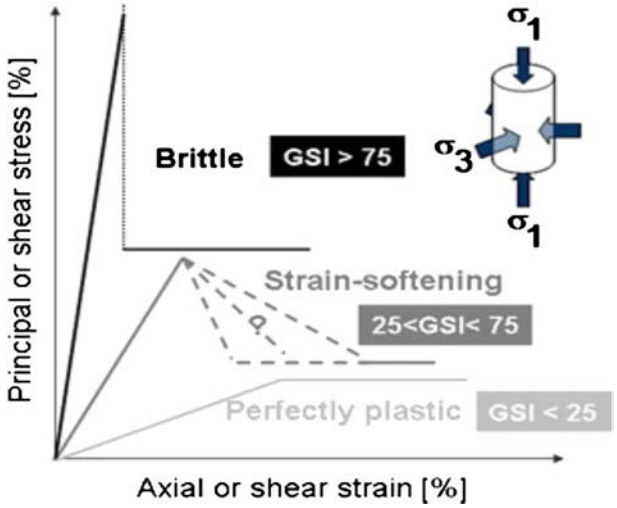

Figure 1. Different post-failure rock mass behaviour modes for rock masses with different geological strength indexes (GSI) [14].

A simplifying assumption in their work was that brittle failure occurred for rock masses characterized by GSI >75 and perfectly plastic behaviour for rock masses with GSI < 25. For a GSI value between 25 and 75, a strain-softening behaviour was assumed. It was also recognized that estimating a 'residual' GSI is not straightforward. For engineering purposes, however, there are cases that defining the post-peak behaviour of a rock mass can have significant impact on geomechanical design.

Stress analysis tools are used to assess the behaviour of a rock mass surrounding an engineering excavation whether it is a borehole, raise, drift, stope, etc. These numerical tools require the use of a constitutive model that describes the behaviour of a rock mass. It is a common practice in rock engineering that the behaviour of the rock mass is defined by a single constitutive relationship irrespective of the size of the engineering work under investigation. On the other hand, it is reasonable to assume that at the scale of a borehole, the behaviour of the rock mass will differ locally from the rock mass behaviour at a larger scale engineering construction (i.e. stope or entire mine). This paper investigates the significance of the way the constitutive behaviour of jointed rock masses is defined at different rock mass sizes and different engineering structures.

Of interest are recent developments in numerical methods, such as the 2D and 3D synthetic rock mass (SRM) approaches [16–19], which can simulate a jointed rock mass and can be used to estimate the strength and deformation of the generated model. A SRM model represents a jointed rock mass as an assembly of fractures superimposed into the rock matrix. If a SRM model is subjected to a load, then new fractures can develop or initiate depending on the imposed stress and strain level. In order to generate a SRM model, it is necessary to capture the geometry of a fracture network. This can be derived from drilling and mapping on site. A statistically based discrete fracture network (DFN) is subsequently introduced in the SRM model. The properties of intact rock and of discontinuities determined from laboratory tests can be directly implemented in the SRM models.

Cundall et al. [20] and Esmaieli et al. [21] used the SRM approach to estimate scale effect on the ultimate strength and elastic behaviour of rock samples. The SRM approach was also employed to simulate the interaction of stress and structure on the stability of vertical excavations in hard rocks, for excavations at deep [22] and shallow depth [23]. Esmaieli et al. [24] focused on applying the SRM technique to estimate the geometrical and mechanical representative elementary volume (REV). The present work is an extension of previous work by the authors in that it addresses the behaviour of different scale SRM samples that are loaded to past their peak strength. It was thus possible to capture the complete stress–strain behaviour of the SRM samples and allowed an insight into the post-peak behaviour of a massive sulphide rock mass. This can contribute to the discussion of whether it may be possible to select a representative constitutive model as a function of the engineering scale of an excavation.

The authors used available geological structural data to generate a representative DFN for the rock mass at Brunswick mine. The generated fracture network was subjected to a random sampling at random locations and in various sample size. The fracture network samples were embedded into 3D bonded particle models (BPMs), representing intact rock matrix, to construct the SRM samples. Finally, the SRM samples were uniaxially loaded to measure their pre-peak and post-peak properties.

2 STRUCTURAL DATA COLLECTION AND ANALYSIS

Brunswick mine, a lead-zinc-copper-silver mine located in north-eastern of New Brunswick, Canada, 26 km south-west of Bathurst was in operation from 1964 until it was closed in April 2013. The ore body at Brunswick mine consists of ten almost sub-parallel massive sulphide lenses striking north– south and dipping 75° to the west. The deposit is a volcanic massive sulphide deposit type hosted by metamorphosed volcaniclastic sediments and tuffs that overly felsic volcanic rocks [25]. The mechanical properties of the massive sulphide are much higher than the meta-sediments. The massive sulphide rock is heavy (specific gravity of 4.3), stiff and strong (uniaxial compressive

strength (UCS) up to 200 MPa), while the meta-sediments are much lighter (specific gravity 2.6) and weaker (UCS up to 70 MPa).

A structural data collection campaign was undertaken at Brunswick mine. Six scanlines were traced on the massive sulphide exposures in the lower mine block. To account for orientation bias, mapping was carried out in different directions. Overall, the rock mass is moderately fractured. The results of fracture mapping identified three fracture sets, two sub-vertical sets and one sub-horizontal set. The sub-vertical fracture sets were oriented relatively perpendicular to each other, striking towards the north–south and east–west directions. The dip, dip direction and the characteristics of each fracture set are summarized in Table I. The Fisher constant K was employed to quantify the dispersion of the orientation data around the mean value. The majority of recorded fractures had two defined terminations; consequently, no correction was made for censoring bias.

Table I. Characteristics of fracture sets,

				Spacing (m)		Trace length (m)	
Set #	Dip (°)	Dip dir (°)	K	Mean	Std.	Mean	Std.
1	89	007	17	1.52	1.8	1.40	0.70
2	89	274	12	1.12	1.0	1.44	0.54
3	17	227	57	1.23	0.8	1.16	0.22

3 A DISCRETE FRACTURE NETWORK (DFN) MODEL FOR THE ROCK MASS

Details of the SRM sample generation for the massive sulphide rock mass at Brunswick mine have been reported in Esmaieli et al. [24]. The major steps of the process are reproduced in the subsequent sections

3.1 DFN model generation and validation

Stochastic 3D DFN models have found many applications in rock engineering, including mining, civil, waste disposal, and reservoir engineering applications. DFN models are developed based on fracture characteristics such as orientation of fracture sets, fracture shape, size, and termination [26]. Mean values and statistical distribution of these fracture characteristics are usually determined by analyzing the results of structural field mapping.

The Fracture-SG code [27] was used for generation of a DFN model for the massive sulphide rock mass at Brunswick mine. This generator employs the Veneziano model for fracture generation. A fracture network of 40 × 40 × 40 m was generated and validated based on the structural data summarized in Table I. Fracture generation was realized, per fracture set basis, using size, intensity and orientation as input. Figure 2 presents a realization of the fracture network with the y-axis representing north. Because DFN models are based on stochastic generation, the model used in this analysis is only one of many possible networks.

The validation procedure comprises of comparison of field structural data and the information resulting from simulated model. Figure 3 shows a comparison between the stereonets of the sampled fractures along the six scanlines and the same virtual scanlines in the 3D DFN model. The distribution of fracture characteristics for simulated fracture network was derived and compared with the distribution of field observed data, using a Kolmogorov–Smirnov test [28]. This includes the distribution of fracture orientation, spacing and trace length of the simulated model.

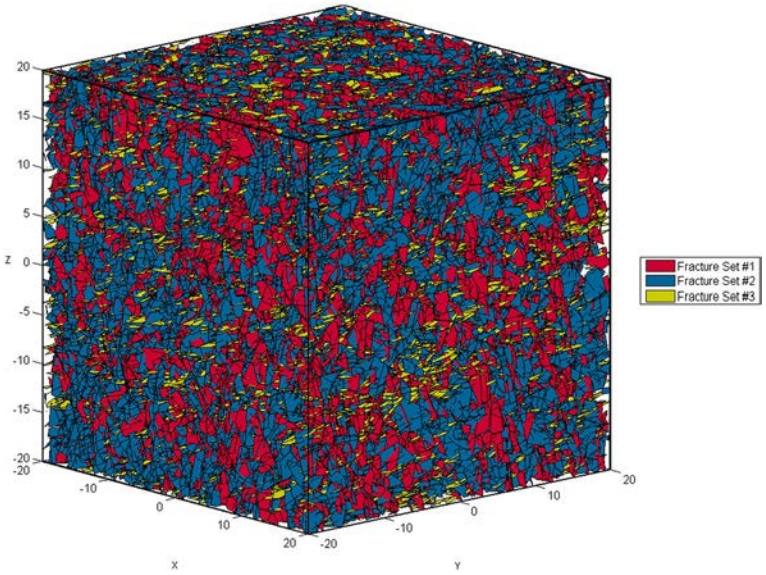

Figure 2. A master DFN model generated for the massive sulphide rock mass, set #1: blue; set #2: yellow; set #3: red.

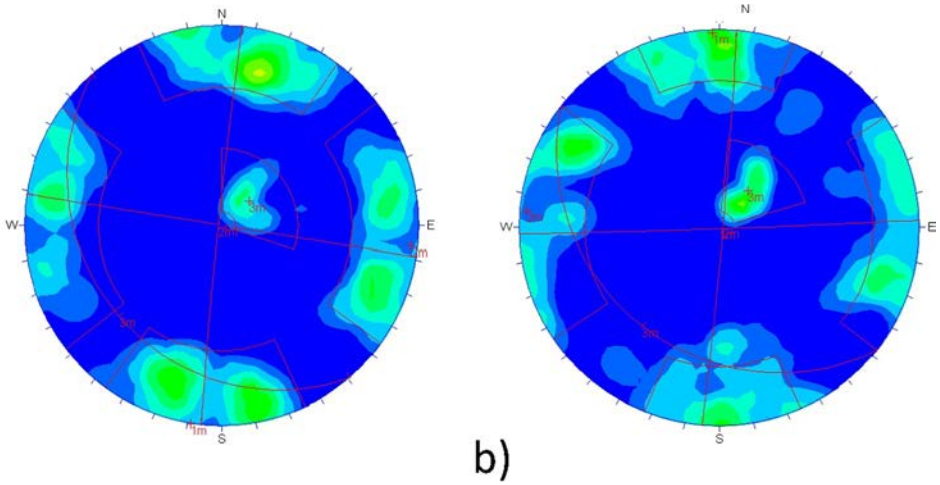

Figure 3. (a) Stereonet constructed from scanline mapping data; (b) stereonet constructed from the virtual scanlines introduced into the DFN model.

3.2 Sampling the DFN model

The constructed DFN model was subjected to random spatial sampling. In all, 40 cubic samples of constant height/width ratio of two were collected. Eight sample sizes of 0.05, 0.1, 0.2, 0.5, 1.5, 3.5, 7.0, and 10.0 m width were selected (Figure 4). This resulted in five random samples per each sample size from within the 'master' volume. Depending on the size of samples and the sampling location within the master volume, a fracture can be completely enclosed or it can be truncated by the sample boundaries.

Different terms are generally used to describe the amount of fracturing of a rock mass. This includes fracture density, intensity and porosity [29]. The volumetric fracture intensity P32 is a very useful measure of rock mass fracturing and is defined as the sum of all fracture area enclosed within a specific volume, divided by that volume. Unlike linear fracture intensity (P10) or areal fracture intensity (P21), the P32 is not a direction-dependent measure of rock mass fracturing. However, it is impossible to obtain the P32 directly from field measurements. The P32 can be obtained from P10

or P21 values measured in the field, using conversion factors. The conversion factors can be developed by DFN simulation. For the purpose of this study, the P32 value of all the DFN samples was measured and summarized in Table II. It can be seen that the variations of the calculated P32 values decrease with the increase of the sample size, and it converge to a mean value of 2.65 m^{-1} for the 7 × 7 × 14 m sample.

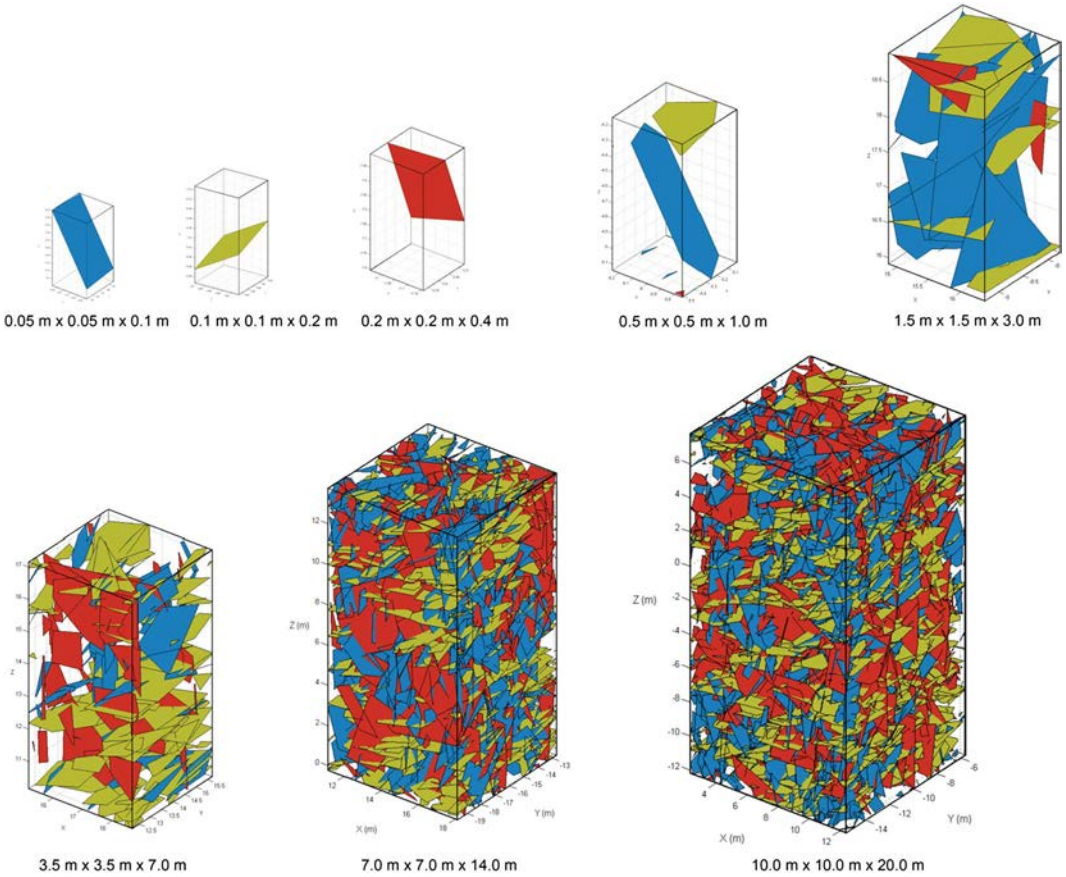

Figure 4. DFN samples of different sizes taken from the master DFN model.

Table II. The volumetric fracture intensity for different DFN samples.

	Volumetric fracture intensity (P_{32}) (m^{-1})						
	DFN sample						
Sample size (m)	S1	S2	S3	S4	S5	Mean	Std.
0.05	20.1	0.00	19.6	0.00	0.00	7.96	10.90
0.1	0.00	5.11	0.00	10.26	5.95	4.26	4.35
0.2	3.76	5.09	0.41	5.51	5.18	3.99	2.10
0.5	5.21	3.18	1.31	1.88	2.53	2.82	1.50
1.5	3.33	2.81	2.08	2.28	1.66	2.43	0.64
3.5	1.97	2.60	2.66	1.84	2.45	2.3	0.37
7.0	2.80	2.40	2.90	2.47	2.70	2.65	0.21
10.0	2.55	2.70	2.45	2.60	2.80	2.62	0.13

4 SYNTHETIC ROCK MASS SAMPLES

A SRM model is defined as a hybrid numerical model constructed by linking the particle flow code (PFC), a distinct element method (DEM) developed by Itasca [30], and a DFN. The SRM model represents a jointed rock mass as an assembly of fractures inserted into a rock matrix and can simulate intact rock failure together with fracture movement. Applying a load on the SRM model results in fracture initiation and propagation. The behaviour of a SRM model is controlled by both the solid rock matrix and the embedded fracture network. The SRM approach was employed to capture the mechanical behaviour of the massive sulphide rock mass.

4.1 Intact rock simulation

A solid rock material was simulated as a BPM using procedures developed by Potyondy and Cundall [31]. A BPM represents an intact rock as packed non-uniform spherical particles that are connected together at their contact points with parallel bonds. The inverse calibration method was used to establish the appropriate micro-mechanical parameters of a BPM that resulted in representative intact rock properties for the massive sulphide rock. This required assigning the mechanical properties of intact rock in a BPM and comparing the results of mechanical properties obtained from laboratory tests to those from computational tests. Table III lists the mechanical properties for the massive sulphide rock at Brunswick mine obtained from laboratory tests to the results from PFC3D numerical experiments. The intact rock samples were generated for eight different sizes corresponding to the DFN model sampling (Figure 5).

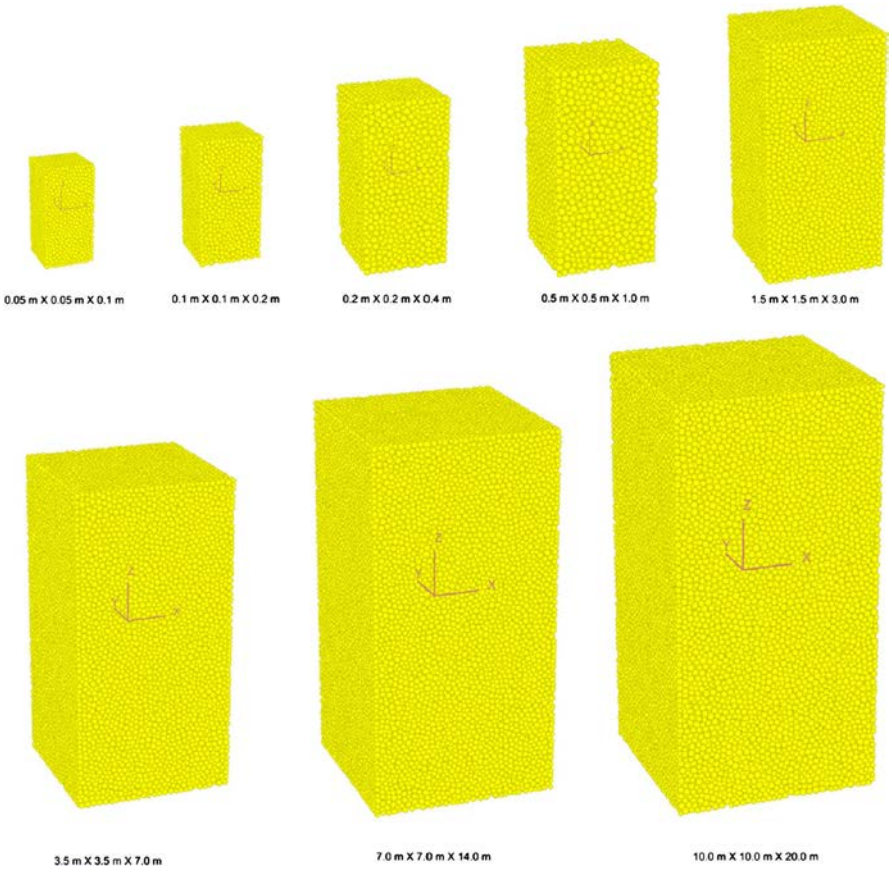

Figure 5. Bonded particle models of intact rock samples.

Table III. Mechanical properties of intact rock and bonded particle models.

Mechanical properties		UCS (MPa)	Elastic modulus (GPa)	Poisson ratio	Specific gravity
Massive sulphide rock		205	104	0.29	4.3
PFC3D	0.05	203	104	0.29	4.3
sample	0.1	204	102	0.29	4.3
size (m)	0.2	205	104	0.27	4.3
	0.5	204	103	0.28	4.3
	1.5	205	104	0.28	4.3
	3.5	204	104	0.27	4.3
	7.0	204	105	0.29	4.3
	10.0	205	103	0.28	4.3

The two common limitations in how PFC manages intact rock simulations include the small ratios of UCS to tensile strength, together with the low internal friction angle of the BPM. Different approaches have been used to counter these limitations [32–34]. More recently, the grain-based approach [35] and the flat-joint contact model [36] have been developed to better match the ratio of UCS to the tensile strength of intact rocks using BPM. However, all of these approaches have been developed in PFC2D and have yet to be successfully implemented in PFC3D.

In this work, the intact rock calibration process has resulted in tensile strength almost ten times the Brazilian strength of the massive sulphide rock (4.8 MPa). Thus, for this investigation, the calibration of the SRM samples relied on the elastic modulus, Poisson's ratio and UCS. This was judged adequate to simulate the stress–strain behaviour of the SRM samples under compression loading. It is recognized that increased confidence in the calibrated model can eventually be achieved by further exploring the potential of flat-joint and grain-based models.

In the current work, the minimum ball radius was selected for each sample based on the sample width. Larger particle sizes were used for larger samples in order to reduce the computation time of the sample testing. Although different particle sizes were used for generation of different sample sizes, all the BPM samples have the same mechanical properties (UCS, elastic modulus, Poisson's ratio). For this purpose, different micro-properties were assigned for the generation of different BPM sample sizes. More detailed information on generation and calibration of the BPMs can be found in Esmaieli et al. [24].

The particle size of samples has limited influence on the SRM strength and deformation results, if the particle size would be considerably smaller than mean joint spacing. This was investigated by using different discretizations (minimum particle radius) for the largest SRM sample (10 × 10 × 20 m) where the difference in strength and deformation results was minimal.

4.2 Simulation of fractures

A BPM can represent a homogeneous rock, or it can be divided into a number of discrete regions or blocks by fractures. The properties of particles and bonds along the fracture planes are usually different than those that exist in the solid part of the model. This work employed the smooth joint model (SJM) to simulate the fractures. The SJM developed by Mas Ivars et al. [37] was chosen as it allows sliding and unravelling of rock blocks along the fracture surface. The SJM was applied to the particle contacts along the fractures to simulate the behaviour of fracture's interface, regardless of local particle contact orientations along the fracture surface.

In the current study, all fractures were assumed to be cohesionless and having an angle of friction of 30°. The calibration process to assign the necessary micro-mechanical properties to the particles along the fracture planes, in order to achieve the desired cohesion and friction angle for fractures, has been described in detail by Esmaieli et al. [24].

4.3 SRM sample generation

The input parameters for the SRM sample generation are intact rock properties, fracture properties and the fracture geometrical characteristics represented by a DFN model. To generate the SRM samples, the fractures of the DFN samples were incorporated into the corresponding BPMs for each sample. In all, 40 SRM samples of eight different sizes were generated. Figure 6 presents one SRM sample of each sample size.

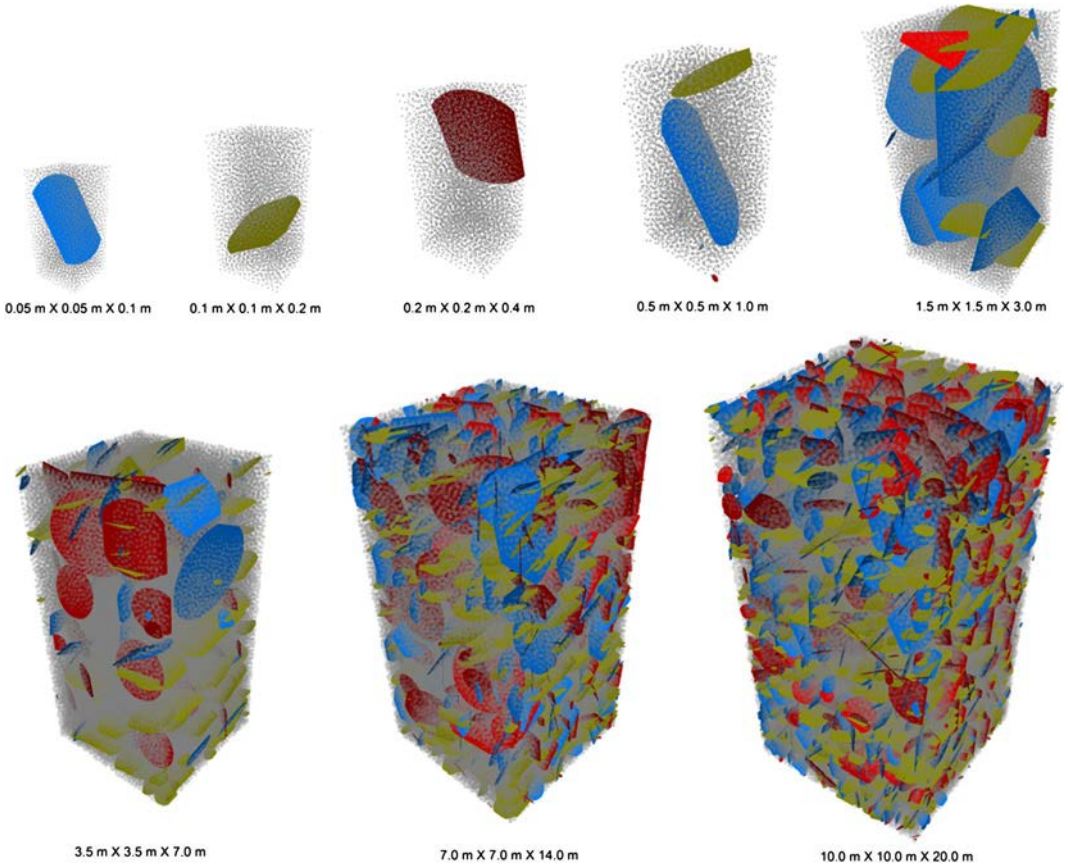

Figure 6. Synthetic rock mass (SRM) samples of different sizes.

4.4 Uniaxial loading of the SRM samples

A series of uniaxial compressive numerical experiments were carried out on the SRM samples recording both pre-peak and post-peak behaviour. Smaller samples (0.05, 0.1, 0.2 and 0.5 m) were loaded by the wall-based loading procedure in PFC3D. In this process, the walls that confine the specimen in the BPM generation were used to load the specimen with the top and bottom walls acting as loading platens. The loading walls are frictionless that can decrease bulking of SRM samples as a result of boundary conditions.

A grip-based procedure was used to load the larger samples. Grip spheres on the top and bottom of each rock sample were identified as plates and moved towards each other, resulting in the desired velocity to the grip spheres. This resulted in loading of the SRM samples from the top and bottom. Consequently, the particles of the loaded samples displaced axially (towards each other) and laterally, until the sample failed. A full stress–strain curve was developed for each SRM specimen.

5 INTERPRETATION OF THE NUMERICAL EXPERIMENTS

A typical stress–strain curve for a strain-softening material (i.e. moderately fractured hard rock masses) is presented in Figure 7. This conceptual stress–strain curve identifies the following stages: elastic zone, yielding zone, brittle zone, softening zone and residual zone. The full stress–strain curve is only obtained using stiff servo-controlled loading rigs [38]. Most commercial stiff servo-controlled testing rigs are limited to small-scale rock samples; consequently, there are very limited experimental data on the complete stress–strain behaviour for large size samples.

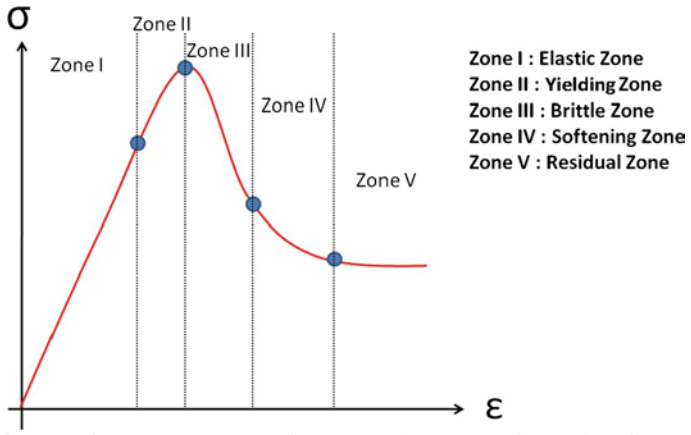

Figure 7. Typical complete stress–strain curve for a strain-softening material.

5.1 Pre-peak mechanical behaviour

The pre-peak mechanical behaviour of a rock can be characterized based on the elastic zone (zone I) and yielding zone (zone II) of a stress–strain curve by recording the elastic modulus and the UCS of the sample. The relationship between the sample size and UCS and elastic modulus of the generated SRM samples has been reported by Esmaieli et al. [24]. It was shown that both the UCS and elastic modulus reduce with increase in sample size. In addition, it was demonstrated that the variation in UCS and elastic modulus diminish with sample size. The mean UCS value of the largest sample size (10 × 10 × 20 m) was approximately 45 MPa, which is close to 20% of the UCS of the intact massive sulphide rock. The mean elastic modulus of the largest sample was approximately 38 GPa, close to 36% of the elastic modulus of the intact rock. Consequently, using statistical tests, it was possible to obtain a REV for the massive sulphide rock mass based on the results of UCS and elastic modulus. The mechanical REV size was found to be the sample size 7 × 7 × 14 m. This is a sample size for which the variation of the volumetric fracture intensity P32 decreases significantly.

5.2 Post-peak mechanical behaviour

The post-peak mechanical behaviour of a fractured rock mass can be characterized based on the zone III, zone IV and zone V of its full stress–strain curve (refer to Figure 7). This includes the estimation of post-peak modulus, brittleness index and residual strength of the rock sample.

Figure 8 shows the full stress–strain curves for different size SRM samples. The cumulative number of micro-cracks developed in each specimen during loading is also plotted on the same graph. In this study, a micro-crack is defined as a bond breakage within the SRM sample. The bonds between spherical balls fail because of both shear and tensile forces. In all of the tested samples, tensil-einduced micro-cracks were more dominant than shear-induced micro-cracks. The cumulative number of micro-cracks in each stage of the compressive test indicates the extent of local damage

in a rock sample, associated with the evolution and propagation of failure within the rock sample. It should be noted that the number of bonds in each sample depends on the number of spherical balls comprising that sample. Larger samples consist larger number of balls and consequently more bonds. Table IV summarizes the number of balls and bonds for the intact samples of each specimen size together with the number of bonds for each SRM sample. Because of the presence of joints in the SRM samples, represented with 'SJM', the number of bonds in the SRM samples is lower than their intact samples.

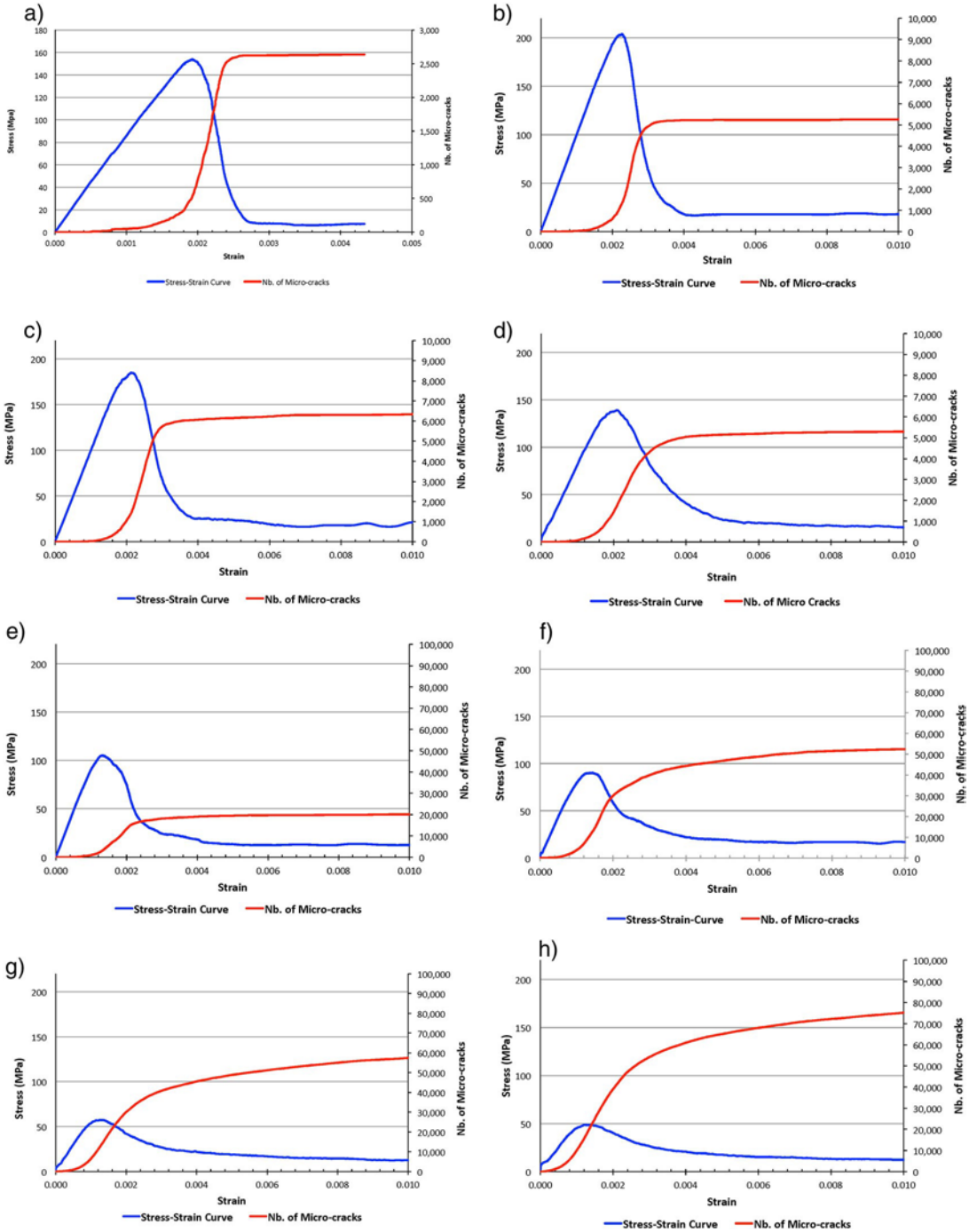

Figure 8. Complete stress–strain curve and cumulative number of micro-cracks for the SRM samples of different width sizes: (a) 0.05 m, (b) 0.1 m, (c) 0.2 m, (d) 0.5 m, (e) 1.5 m, (f) 3.5 m, (g) 7.0 m, (h) 10.0 m.

Figure 8 illustrates that the majority of stress-induced micro-cracks develop within the samples when the loading condition is between yielding zone (zone II) and strain-softening zone (zone IV). In the majority of tested SRM samples, only 20 to 30% of the total cumulative number of micro-cracks developed before the UCS. For smaller sample sizes (0.05 to 0.5 m), once the residual strength was reached, the number of micro-cracks remains almost constant. For the larger sample sizes (1.5 to 10 m), although the rate of micro-crack development in the samples decreased, following the strain-softening zone (zone IV), micro-cracks continued to develop until the sample was in the residual zone (zone V). This can be explained by a relatively simpler failure path for smaller samples than more complex failure plane in the larger SRM samples.

Table IV. Number of particles and bonds in different sample sizes.

Sample size (m)	No. of balls	Minimum ball radius (cm)	No. of bonds					
				SRM sample				
			Intact sample	S1	S2	S3	S4	S5
0.05	5512	0.16	14 818	14 374	14 818	14 376	14 818	14 818
0.1	6063	0.31	16 386	16 386	16 076	16 386	15 887	16 048
0.2	6689	0.6	18 185	17 735	17 700	18 165	17 512	17 584
0.5	8228	1.4	22 275	20 535	21 178	21 997	20 543	21 448
1.5	39 014	2.5	111 110	101 417	103 173	104 998	104 508	106 393
3.5	92 300	3.6	267 001	242 454	235 140	233 600	244 178	236 587
7.0	115 455	7.0	335 182	255 983	267 195	263 887	265 930	259 357
10.0	142 376	10.0	414 754	301 121	297 936	304 116	298 746	292 034

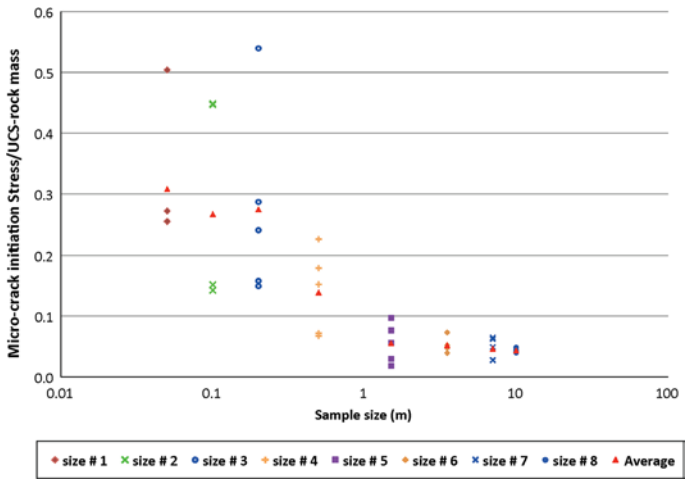

Figure 9. Influence of specimen size on the ratio of micro-crack initiation stress/UCS.

In reviewing the results plotted in Figure 8, it is observed that smaller samples appear to be more brittle than larger samples. It is possible that the behaviour of smaller samples is better described by strength weakening than strain softening. The larger SRM samples are less brittle.

The massive sulphide rock mass at Brunswick mine can be described by a GSI close to 75. If one applies the guidelines by Alejano et al. [14], a rock mass of GSI = 75 is expected to be brittle. This would appear appropriate given the numerical experiments on the small SRM samples. It is not, however, in close agreement with the modelling results for larger samples where strain-softening behaviour seems to be dominant.

Figure 9 illustrates the relationship between the ratio of micro-crack initiation stress/UCS of each sample versus the sample size. The results indicate that the threshold stress level, for micro-crack

initiation, decreases with the sample size. This implies that micro-cracks initiate, in larger samples, at lower stress levels. In addition, the variation of stress level decreases with sample size. It can be seen that for a sample size greater than 1.5 m, the ratio reaches a plateau, suggesting that for sample sizes larger than 1.5 m size, crack initiation will start at the same stress level.

5.2.1 Brittleness index.

Tarasov [39] proposed a brittleness index k, to quantify rock brittleness in compression conditions of $\sigma_1 > \sigma_2 = \sigma_3$ for intact rock. This index is based on the elastic energy accumulated in the rock during loading and the portion of this energy that cause failure development in the post-peak phase.

$$k = \frac{dW_r}{dW_e} = \frac{E-M}{M} \quad (1)$$

where $dW_r = \frac{d\sigma^2(E-M)}{2EM}$ is the rupture energy; $dW_e = \frac{d\sigma^2}{2E}$ is the accumulated elastic energy available for the rupture process; $E = \frac{d\sigma}{d\varepsilon}$ is the unloading elastic modulus; $M = \frac{d\sigma}{d\varepsilon}$ is the post-peak modulus.

The parameters in Eqn 1 can be determined from the complete stress–strain curves. Tarasov [39] demonstrated the variation in brittleness index with variation of complete stress–strain curves (Figure 10).

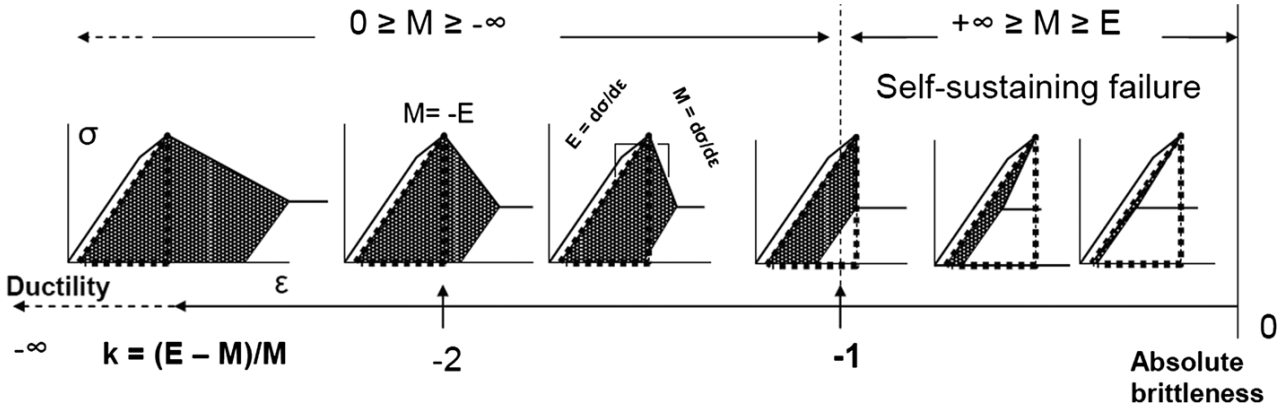

Figure 10. Variation of brittleness index (k) with characteristic shape of complete stress–strain curves [39].

The brittleness index k increases from left to right. In this figure, it was assumed that pre-peak parts of the curves are the same. The brittleness index is negative ranging from $-\infty < k < 0$ The brittleness index proposed by Tarasov [39] was calculated for the SRM samples in this investigation. Figure 11 presents the results of post-peak modulus (M) versus sample size. The graph shows that the mean post-peak modulus (M) and its variance decrease with sample size. The post-peak modulus of the intact rock sample was measured as 260 GPa. The average post-peak modulus of the 10 × 10 × 20 m rock mass sample (size #8) was approximately 11 GPa. This is close to 4% of the post-peak modulus of the intact rock and can have significant implications for design purposes.

Figure 12 shows the variation of brittleness index k versus specimen size. It is illustrated that the brittleness index decreases with sample size. The variance of measured values remains relatively high for all sample sizes. The brittleness index of the intact rock sample was measured as 1.4. The brittleness index for the largest sample size (size #8) was $4.7 < k < 4.2$. This is more than three times the brittleness index of the intact rock. This implies that the larger rock mass samples are less brittle than smaller sample sizes.

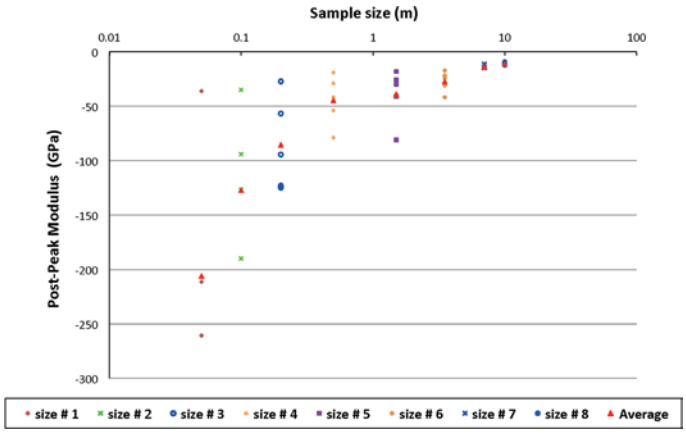

Figure 11. Influence of specimen size on the post-peak modulus of SRM samples.

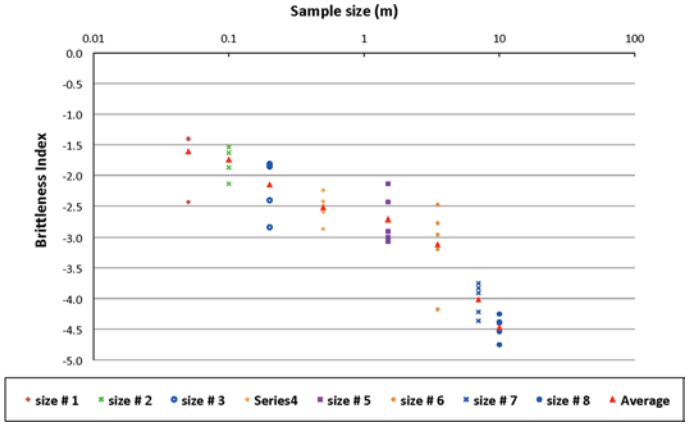

Figure 12. Influence of specimen size on the brittleness index of the SRM samples.

5.2.2 Residual strength.

Figure 13 displays the influence of specimen size on the ratio of the residual strength per the UCS of intact rock (i.e. BPM without an embedded DFN). The ratio of SRM residual strength/UCS-intact rock varies from less than 1% to more than 10%. These variations are caused by the presence or absence of joints within the generated SRM samples. A smaller variation was observed for larger rock mass samples as they approach the REV size (7 × 7 × 14 m). The majority of tested samples have a residual strength between 5 and 15 MPa. While the variability of the residual strength values decreased with sample size, the mean residual strength of the samples slightly increases with sample size. For the largest sample size (size #8), the mean residual strength is about 12 MPa. This is close to 6% of the intact rock UCS. The peak strength of the largest sample was 45 MPa, approximately 20% of the intact rock UCS. This implies that for this sample size (size #8), the strength has declined 14% from peak to residual with respect to the intact rock UCS.

The ratio of residual strength to the peak strength (UCS-rock mass) of the SRM samples was plotted against the sample sizes (Figure 14). The results suggest that the ratio of residual strength/UCS-rock mass increases with sample size. The ratio rises from 5–8% for the smallest sample size (size #1) to 24–30% for the largest rock mass samples (size #8). The graph indicates that by knowing the peak UCS of the rock mass, it is possible to estimate the residual strength of

the rock mass. These results are similar to the findings of Cai et al. [11] where GSI-rm was related to GSI-residual.

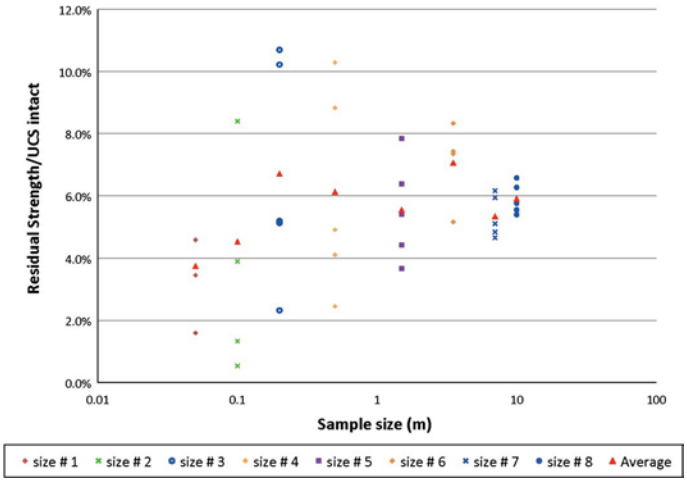

Figure 13. Influence of specimen size on the ratio of residual strength/UCS-intact rock of the SRM sample.

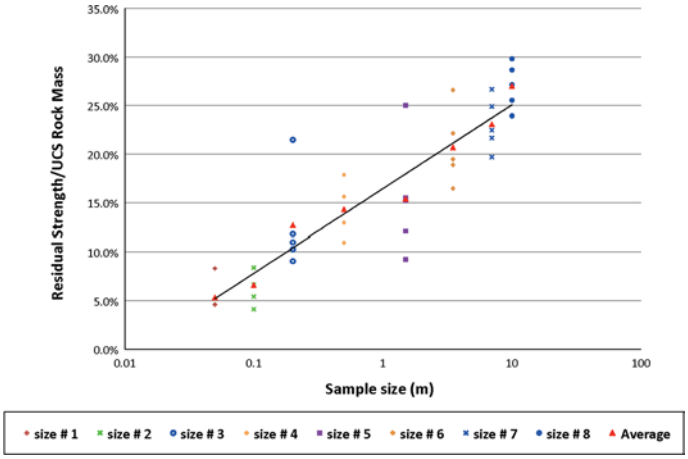

Figure 14. Influence of specimen size on the ratio of residual strength/peak UCS-rock mass of the SRM samples.

According to Alejano et al. [14], the residual strength of a rock mass characterized by GSI 75< should be 60% of the UCS-rm. This is higher than results obtained by the SRM modelling that shows a ratio of 27% for the largest sample size.

The coefficient of variation (CV), the ratio of the standard deviation to the mean value, was calculated for both pre-peak and post-peak properties of the rock mass. The pre-peak and post-peak properties of the rock mass samples are listed in Table V and Table VI, respectively. The CV of the post-peak modulus, the residual strength, the UCS and the elastic modulus was plotted against sample size, Figure 15. The results indicate that the CV values of both pre-peak and post-peak mechanical properties converge as the sample size increase. Min and Jing [40] stated that the REV size for a given rock mass can be estimated based on a chosen acceptable variation. Using a 20% variation for CV as an acceptable variation, the REV size for both pre-peak and post-peak properties would be 7 × 7 × 14 m sample size (size #7). This implies that the REV size for the pre-peak mechanical properties is the same for the post-peak properties.

Table V. Results of pre-peak mechanical properties.

Sample size (m)	UCS of intact rock (MPa)	Elastic modulus of intact rock (GPa)	Uniaxial compressive strength of SRM samples (MPa)					Mean (MPa)	Std. (MPa)	Elastic modulus of SRM samples (GPa)					Mean (GPa)	Std. (GPa)
			S1	S2	S3	S4	S5			S1	S2	S3	S4	S5		
0.05	203	104	154	203	39	203	203	160.4	71.1	87	104	52	104	104	90.2	22.5
0.1	204	102	204	66	204	120	20	122.8	82.1	102	82	102	80	40	81.2	25.3
0.2	205	104	95	185	203	22	117	124.4	72.8	80	100	104	50	81	83.0	21.4
0.5	204	103	28	139	192	64	59	96.4	67.2	27	81	98	67	54	65.4	26.9
1.5	205	104	30	58	91	105	141	85.0	42.7	26	52	62	78	92	62.0	25.2
3.5	204	104	90	57	65	91	54	71.4	17.8	62	55	47	68	39	54.2	11.5
7.0	204	105	38	54	39	58	50	47.8	8.9	33	44	37	49	42	41.0	6.2
10.0	205	103	45	49	47	39.5	43	44.7	3.6	38	42	41	36	35	38.4	3.0

Table VI. Results of post-peak mechanical properties.

Sample size (m)	Post-peak modulus of SRM samples (GPa)					Mean (GPa)	Std. (GPa)	Residual strength of SRM samples (MPa)					Mean (MPa)	Std. (MPa)
	S1	S2	S3	S4	S5			S1	S2	S3	S4	S5		
0.05	−211	−260	−36	−260	−260	−206	97	7.0	9.3	3.2	9.3	9.3	7.6	2.6
0.1	−190	−94	−190	−127	−35	−127	66	17.1	2.7	17.1	7.9	1.1	9.2	7.7
0.2	−57	−123	−125	−27	−95	−85	43	10.4	21.8	20.8	4.7	10.6	13.7	7.4
0.5	−19	−55	−89	−42	−28	−47	27	5.0	18.0	21.0	10.0	8.4	12.5	6.7
1.5	−18	−24	−60	−41	−81	−45	26	7.5	9.0	13.0	16.0	13.0	11.7	3.4
3.5	−42	−17	−24	−31	−22	−27	10	17.0	15.1	14.3	15.0	10.5	14.4	2.4
7.0	−12	−15	−11	−15	−15	−14	2	9.4	12.1	10.4	12.5	9.8	10.9	1.4
10.0	−12	−12	−12	−11	−10	−11	1	13.4	11.7	12.7	11.3	11.0	12.0	1.0

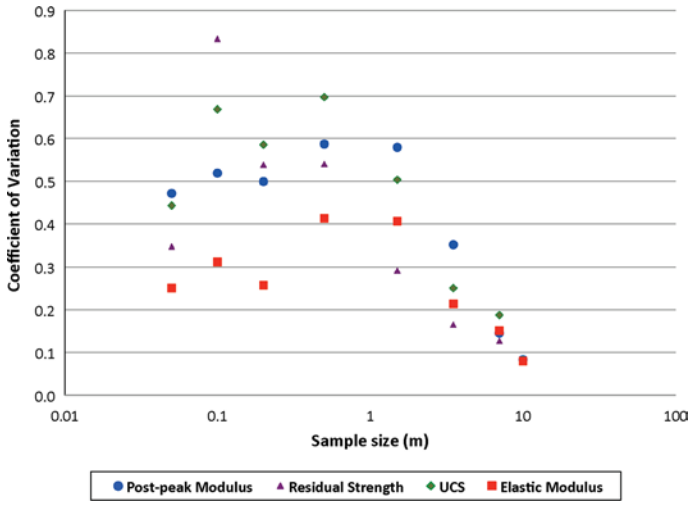

Figure 15. Coefficient of variation versus sample size.

6 CONCLUSIONS

Capturing the full stress–strain behaviour of fractured rock masses including the pre-peak and post-peak behaviour is important for the analysis and design of support in underground excavations, stope design and mine sequencing. The SRM approach was successfully used for quantification of pre-peak and post-peak behaviour of a massive sulphide rock mass at Brunswick mine. Field data were collected to generate a representative DFN model for the rock mass. The fracture network was randomly sampled to take eight different sample sizes varying from 0.05 × 0.05 × 0.1 m to 10 × 10 × 20 m. The DFN samples were linked with BPMs to construct the SRM samples. The generated samples were uniaxially loaded to capture full stress–strain curve for each specimen.

The pre-peak portion of the stress–strain curves for the SRM samples showed a reduction of the UCS and elastic modulus of the rock mass with increasing of the sample size. In addition, variation of the UCS and elastic modulus values decreases as sample size increases. The post-peak portion of the stress–strain curves indicated that the rock mass behaviour changes from a brittle manner to a strain-softening manner as the sample size increases. This is different from common empirical approaches where very good quality rock mass would assume to behave in a brittle manner.

For rock masses at the scale of a large engineering work (tunnel, stope, etc.), for the Brunswick mine massive sulphide case study, the residual strength defined to be equal to 27% of the peak

UCS-rm. These findings have important ramifications in the use of elasto-plastic numerical models for the design of underground excavations.

Measuring the volumetric fracture intensity (P32) of the DFN samples indicated that as the sample size increases, the variation in calculated P32 decreases significantly and it converges to a mean value equal to the fracture intensity of the master DFN volume. Using the CV of the pre-peak and post-peak properties of the SRM samples, the REV size of the rock mass was determined. The REV size for both the pre-peak and post-peak mechanical properties was determined to be equal to 7 × 7 × 14 m. This is the size beyond which the variations of the volumetric fracture intensity P32 decrease significantly.

ACKNOWLEDGEMENTS

The authors would like to acknowledge the support of the Natural Science and Engineering Research Council of Canada (NSERC) and Brunswick mine of Xstrata Zinc.

REFERENCES

1. Hoek E, Kaiser PK, Bawden WF. Support of underground excavations in hard rock. Balkema, Rotterdam, 1995; 300.
2. Bieniawski ZT. Engineering rock mass classifications. Wiley: New Tork, 1989; 251.
3. Barton NR. Some new Q-value correlations to assist in site characterization and tunnel design. International Journal of Rock Mechanics and Mining Sciences 2002; 39(2):185–216. doi:10.1016/s1365-1609(02)00011-4.
4. Halakatevakis N, Sofianos AI. Strength of a blocky rock mass based on an extended plane of weakness theory. International Journal of Rock Mechanics and Mining Sciences 2010; 47:568–582.
5. Cai M, Morioka H, Kaiser PK, Tasaka Y, Kurose H, Minami M, Maejima T. Back-analysis of rock mass strength parameters using AE monitoring data. International Journal of Rock Mechanics and Mining Sciences 2007a; 44 (4):538–549.
6. Dinc OS, Sonmez H, Tunusluoglu C, Kasapoglu KE. A new general empirical approach for the prediction of rock mass strengths of soft to hard rock masses. International Journal of Rock Mechanics and Mining Sciences 2011; 48(4):650–665.
7. Akin M. Slope stability problems and back analysis in heavily jointed rock mass: a case study from Manisa, Turkey.
Rock Mechanics and Rock Engineering 2013; 46(2):359–371.
8. Rummel F, Fairhurst C. Determination of the post-failure behaviour of brittle rock using a servo-controlled testing machine. Rock Mechanics and Rock Engineering 1970; 2(4):189–204.
9. Simon R, Aubertin M, Deng D. Estimation of post-peak behaviour of brittle rocks using a constitutive model for rock joints. In 56th Canadian Geotechnical Conf., Winnipeg, Manitoba, Sep. 29th-Oct 2nd 2003.
10. Crowder JJ, Bawden WF. The Field-Scale Rock Mechanics Laboratory: Estimation of Post-Peak Parameters and Behaviour of Fractured Rock Masses. Golden Rocks 2006, The 41st U.S. Symposium on Rock Mechanics (USRMS), June 17–21, 2006, Golden, CO.
11. Cai M, Kaiser PK, Tasaka Y, Minami M. Determination of Residual Strength Parameters of Jointed Rock Masses Using the GSI System. International Journal of Rock Mechanics and Mining Sciences 2007b; 44(2):247–265. doi:10.1016/j.ijrmms.2006.07.005.
12. Andrieux P, Hudyma M, O'Connor C, Li H, Cotesta L, Brummer R. Calibration of large-scale three-dimensional non-linear numerical models of underground mines using microseismic data. In proceeding of the 1st International FLAC/DEM Symposium, 25–27 August 2008, MN, USA.
13. Alejano LR, Rodriguez-Dono A, Alonso E, Fdez-Manín G. Ground reaction curves for tunnels excavated in different quality rock masses showing several types of post-failure behaviour.

Tunnelling and Underground Space Technology 2009; 24(6):689–705. DOI: 10.1016/j.tust.2009.07.004.

14. Alejano LR, Alonso E, Rodríguez-Dono A, Fernández-Manín G. Application of the convergence-confinement method to tunnels in rock masses exhibiting Hoek–Brown strain-softening behaviour. International Journal of Rock Mechanics and Mining Sciences 2010; 47(1):150–160. doi:10.1016/j.ijrmms.2009.07.008.

15. Cheng C. Influence of discontinuities on post-peak behaviour of rock in uniaxial compressive test by numerical study. Int. Conference on Multimedia Technology, 26–28 July 2011.

16. Pine RJ, Coggan JS, Flynn ZN, Elmo D. The development of a new numerical modelling approach for naturally fractured rock masses. Rock Mechanics and Rock Engineering 2006; 39(5):395–419.

17. Elmo D, Stead D. An integrated numerical modelling discrete fracture network approach applied to the characterization of rock mass strength of naturally fractured pillars. Rock Mechanics and Rock Engineering 2010; 43(1):3–19.

18. Pierce M, Mas Ivars D, Cundall PA, Potyondy D. A synthetic rock mass model for jointed rock. Proceedings of the

first CA-US rock mechanics symposium, Vancouver, 2007; 341–349.

19. Mas Ivars D, Pierce M, Darcel C, Reyes-Montes J, Potyondy DO, Young P, Cundall PA. The synthetic rock mass approach for jointed rock mass modeling. International Journal of Rock Mechanics and Mining Sciences 2011; 48 (2):2019–244. doi:10.1016/j.ijrmms.2010.11.014.

20. Cundall P, Pierce ME, Mas Ivars D. Quantifying the size effect of rock mass strength. Proceeding of the 1st Southern Hemisphere Int. Rock Mech. Symposium, 16–19 September 2008, Perth, Australia.

21. Esmaieli K, Hadjigeorgiou J, Grenon M. Estimation of synthetic rock mass strength accounting for sample size. Proceeding of Int. Conf. On Rock Joints and Jointed Rock Masses, 7–8 January 2009, Tucson, Arizona.

22. Esmaieli K, Hadjigeorgiou J, Grenon M. Stability analysis of the 19A ore pass at Brunswick Mine using two-stage numerical modeling approach. Rock Mechanics and Rock Engineering 2013; 46(6):1323–1338. doi:10.1007/s00603013-0371-1.

23. Hadjigeorgiou J, Esmaieli K, Grenon M. Stability analysis of vertical excavations in hard rock by integrating a fracture system into a PFC model. Tunnelling and Underground Space Technology 2009; 24:296–308.

24. Esmaieli K, Hadjigeorgiou J, Grenon M. Estimating geometrical and mechanical REV based on synthetic rock mass models at Brunswick Mine. International Journal of Rock Mechanics and Mining Sciences 2010; 47(6):915–926. doi:10.1016/j.ijrmms.2010.05.010.

25. Luff W. Geology of Brunswick No. 12 Mine. CIM Bulletin 1977; 70(782):109–119.

26. Dershowitz WS, Einstein HH. Characterizing Rock Fracture Geometry with Fracture System Models. Rock Mechanics and Rock Engineering 1988; 21:21–51.

27. Grenon M, Hadjigeorgiou J. Fracture-SG. A fracture system generator software package, 2008, Version 2.17.

28. Mardia KV. Statistics of Directional Data. Academic Press: London-New York, 1972.

29. Mauldon M, Dershowitz W. A multi-dimensional system of fracture abundance measures. In Geological Society of America Annual Meeting, Summit 2000, November 13–16 2000, Reno, Nevada, USA.

30. Itasca. Particle Flow Code, PFC2D/3D-V.4.0. Consulting Group, Inc: Itasca, 2008.

31. Potyondy D, Cundall PA. A bonded particle model for rock. International Journal of Rock Mechanics and Mining Sciences 2004; 41(8):1329–1364.

32. Ting JM, Khwaja M, Larry R. An ellipse-based discrete element model for granular materials. International Journal for Numerical and Analytical Methods in Geomechanics 1993; 21:6013–6623.

33. Fakhimi A. Application of slightly overlapped circular particles assembly in numerical simulation of rocks with high friction angles. Engineering Geology 2004; 74:129–138.

34. Cho N, Martin CD, Sego DC. A clumped particle model for rock. International Journal of Rock Mechanics and Mining Sciences 2007; 44:997–1010.

35. Bahrani N, Potyondy D, Pierce M, Simulation of Brazilian test using PFC2D grain-based model. In RockEng 2012, 21st Canadian Rock Mechanics Symposium, May, 2012, Edmonton, Canada.

36. Potyondy DO. The bonded-particle model as a tool for rock mechanics research and application: current trends and future directions. In 7th Asian Rock Mechanics Symposium, 15–19 October 2012, Seoul, Korea.

37. Mas Ivars D, Potyondy D, Pierce M, Cundall P. The smooth-joint contact model. In 8th World Congress on Computational Mechanics, 5th European Congress on Computational Methods in Applied Sciences and Engineering, Jun 30Jul 5, 2008, Venice, Italy.

38. Hudson JA, Brown ET, Fairhust C. Optimizing the control of rock failure in servo-controlled laboratory test. Journal of Rock Mechanics 1971; 3(4):217–224.

39. Tarasov BG. Superbrittleness of rocks at high confining pressure. In proceeding of the fifth Int. Seminar on Deep and High Stress Mining, 6–8 October 2010, Santiago, Chile.

40. Min KB, Jing L. Numerical determination of the equivalent elastic compliance tensor for fractured rock masses using the distinct element method. International Journal of Rock Mechanics and Mining Sciences 2003; 40(6):795–816.